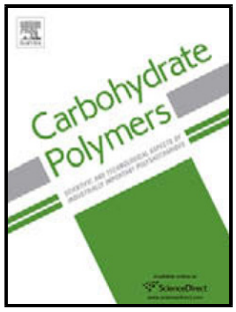

Title: Mechanism and structure studies of cinnamaldehyde/cyclodextrins inclusions by computer simulation and NMR technology

Authors: Qiaomei Sun, Peixiao Tang, Ludan Zhao, Hongyu Pu, Yuanming Zhai, Hui Li

PII: S0144-8617(18)30441-7
DOI: https://doi.org/10.1016/j.carbpol.2018.04.055
Reference: CARP 13509

To appear in:

Received date: 26-1-2018
Revised date: 11-4-2018
Accepted date: 14-4-2018

Please cite this article as: Sun, Qiaomei., Tang, Peixiao., Zhao, Ludan., Pu, Hongyu., Zhai, Yuanming., & Li, Hui., Mechanism and structure studies of cinnamaldehyde/cyclodextrins inclusions by computer simulation and NMR technology.*Carbohydrate Polymers* https://doi.org/10.1016/j.carbpol.2018.04.055

Mechanism and structure studies of cinnamaldehyde/cyclodextrins inclusions by computer simulation and NMR technology

Qiaomei Sun[a], Peixiao Tang[a*], Ludan Zhao[a], Hongyu Pu[a], Yuanming Zhai[b]*, and Hui Li[a]

[a] *School of Chemical Engineering, Sichuan University, Chengdu 610065, China*

[b] *Analytical & Testing Center, Sichuan University, Chengdu 610064, China*

*Corresponding author. **Address:** College of Chemical Engineering, Sichuan University, Chengdu, Sichuan, China. **Tel.:** +86 028 85405220; **Fax:** +86 028 85401207.

E-mail address: tangpeixiao@126.com (Peixiao Tang)； yuanmingzhai@scu.edu.cn (Yuanming Zhai)

Highlights

- Inclusion mechanisms and structures of CNMA-CDs were investigated.
- Docking and molecule dynamics predicted detailed inclusion information.
- The inclusion abilities followed the order: DM > HP > β-CD.
- The benzene ring of CNMA inserted into hydrophobic cavity of CDs.
- The solubility and dissolution rate of CNMA were improved after inclusion.

Abstract

This work aims to explore the inclusion mechanism and structure of cinnamaldehyde

(CNMA) and cyclodextrins (CDs), and to provide some theoretical information for the application of CNMA and its inclusion. In this study, we prepared three kinds of inclusion and investigated the mechanism and structure by theory and experiment. Molecular docking and dynamical simulations presented a stable 1:1 inclusion complex and the visual structure model. The structural features indicated that the benzene ring of CNMA was enclosed in the hydrophobic cavity of CDs, which were consistent with the results of ^{1}H-NMR, 2D-ROESY, Fourier transform infrared spectroscopy. The inclusion mechanism studies showed that the inclusion process was driven mainly by enthalpy with the binding constant following the order of DM (dimethyl) > HP (hydroxypropyl) > β-CD. Moreover, the inclusion complex showed an advantageous water solubility and dissolution rate compared with CNMA.

Key words: Cinnamaldehyde; Cyclodextrin; Inclusion mechanism; Structure; Molecule dynamical simulation

1. Introduction

Cinnamaldehyde (CNMA, **Fig. 1**) is a component of essential oils derived from cassia, which is utilized in several products, including perfumes, essences, and food preservatives. Moreover, the 50% lethal concentration of CNMA was 62 μM for human breast cancer cell MCF-7 indicating potential anticancer bioactivity (Nagle et al., 2012). Administration 20 mg/kg orally for 2 months showed significant improvement for diabetic rats, which showed the antidiabetes bioactivity of CNMA

(Anand, Murali, Tandon, Murthy, & Chandra, 2010). And antithrombus bioactivity of CNMA was revealed when the mortality rate of collagen-epinephrine-induced acute pulmonary thromboembolism effectively reduced with oral administration 250 mg/kg in mice (Huang, Wang, Luo, Xie, & Shi, 2007). However, CNMA is highly volatile, oil liquid and therefore exhibits poor aqueous solubility and stability under ambient temperature. This property is the main factor hindering the application and development of CNMA. Several studies have explored various methods, including α-cyclodextrin inclusion, corn starch inclusion, and microcapsules, to improve the solubility properties of CNMA (Chun, Jo, Bjrapha, Choi, & Min, 2015; Makwana, Choudhary, Dogra, Kohli, & Haddock, 2014; Tian et al., 2013).

Cyclodextrin (CD) is an efficient material to improve physicochemical properties of guest through the inclusion due to its biocompatibility, relatively non-toxicity, and low price (Carrier, Miller, & Ahmed, 2007). The inclusion technology has been widely used in food industries. For example, researchers have investigated the inclusion structure and properties between food additives and cyclodextrins (Castro et al., 2016; Fernándezgarcía & Pérezgálvez, 2017; Zeynep, Semran Ipek, Engin, & Tamer, 2016). These literatures have used cyclodextrin to improve the stability and release rate of food additives in different ways, to expand the application range and field of food additives. Hence, the studies of the mechanism and structure of the inclusion is of great importance to clarify and define the inclusion process.

Many methods ranging from computer simulations to experimental approaches

are available for characterizing the structure and mechanism between guest and cyclodextrins (Abdolmaleki, Ghasemi, & Ghasemi, 2017; Li et al., 2015). Nuclear magnetic resonance (NMR) is the most widely used because it provides reliable chemical information (Pessine, Calderini, & Alexandrino, 2012). ^{1}H-NMR, NOE experiments (ROESY and NOESY), and solid-state NMR are the common methods used for studying inclusions in the literatures (Ferro et al., 2017; Liscieplak, Sitkowski, & Kolodziejski, 2014). Moreover, the development of computer technologies has rendered computer simulation a key strategy for inclusion research, including docking (Zhang, Liu, Yang, Chen, & Jiao, 2017) and dynamic simulation (Li et al., 2015). Therefore, the combination of experimental methods and the theoretical simulation could benefit to obtain reliable information about inclusion mechanism and structural characteristic.

In this study, β-cyclodextrin (β-CD), hydroxypropyl-β-cyclodextrin (HP-β-CD), and dimethyl-β-cyclodextrin (DM-β-CD) (**Fig. 1**) were chosen to prepare an inclusion complex with CNMA. This study aimed to gain insight into the structure and mechanism of the inclusion complex by performing computer simulations and experiments. Molecular docking and dynamics simulation were conducted to intuitively predict the combination mode and the inclusion structure. The inclusion mechanism (including inclusion ratio, apparent binding constant, and thermodynamic parameters) were determined through NMR and isothermal titration calorimetry (ITC). The characterization of structure and morphology of the CNMA-CDs inclusion

complex were studied by 2D-ROESY and solid-state characterization method. And, the encapsulation efficiency, aqueous solubility, and dissolution were investigated for all inclusion complexes. The results of this study would contribute to the application and development of CNMA in the food and pharmaceutical industries.

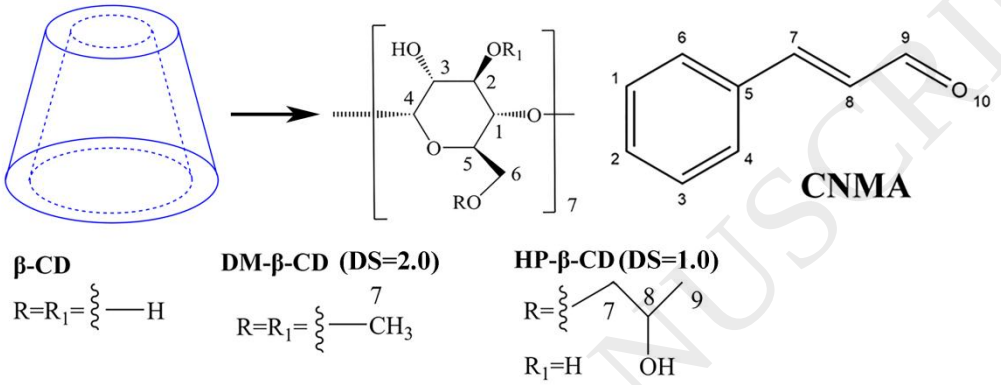

Fig. 1. Structure and atom labels of CDs and CNMA.

2. Experimental

2.1. Materials and reagents

CNMA was obtained from J&K Scientific Ltd. (Beijing, China). β-CD (F_W = 1135, purity ≥ 98%), DM-β-CD (DS = 2.0, F_W = 1331.39, purity ≥ 98%), and HP-β-CD (DS = 1.0, F_W= 1541.54, purity ≥ 98%) were acquired from Chengdu Kelong Chemical Co., Ltd. (Chengdu, China). DMSO-d6 was purchased from J&K Scientific Ltd. (Beijing, China). The other reagents and chemicals used were of analytical reagent grade. Tri-distilled water was used throughout the experiment.

2.2. Preparation of inclusion complexes

To prepare the inclusion complexes, β-CD/DM-β-CD/HP-β-CD was combined with CNMA at a 1:1 molar ratio (Ponce Cevallos, Buera, & Elizalde, 2010). The mixed solution intermittently reacted ultrasonically for 0.5 h and magnetically stirred at 60 ℃ for 8 h. The reaction process maintained the sealing state to prevent the volatilization loss of CNMA. Subsequently, the reaction solution was filtered to remove solid residues and fully frozen in a refrigerator at -20 ℃. The final complexes obtained by drying in a laboratory vacuum freeze dryer for two days, and the temperature of the condensing plate was -60 ℃. The inclusion complexes were protected from light in a dry place. For comparison, corresponding binary physical mixtures with the same ratio at 1:1 were prepared by simply mixing CNMA and CD for 10 min by using a vortex blender.

2.3. Molecular docking and dynamics simulations

The 3D structure of CNMA was built and optimized from ChemBio Office 2012. The 3D cyclodextrin structures were downloaded from Cambridge Structural Database (Ref. code: BCDEXD03 for β-CD; Ref. code: BOYFOK03 for DM-β-CD), and all attached water molecules were removed. The structure of HP-β-CD was established on the basis of β-CD, and optimized by ChemBio3D Ultra through MM2 molecular mechanics method. Molecular docking and MD simulations were performed on YASARA v16.7.22 with AMBER14 force field (Krieger, Darden, Nabuurs, Finkelstein, & Vriend, 2004). Partial atomic charges of CNMA were computed using the AM1-BCC model, and counter ions (Na^+ or Cl^-) were added to

obtain a charge-neutral system. Simulations in explicit water were conducted at a constant temperature (298.15 K) in pH 7.4 after initial energy minimization procedures. Periodic boundary conditions were applied to the system. The long-range Coulomb interactions were applied using particle-mesh Ewald (PME) summation and a cut-off of 8.0 Å. The system with the lowest energy was analyzed within the docking results, and chosen to run MD simulations. Simulations were carried out using a pre-defined macro (md_run) within YASARA package. Multiple time steps were used in the simulation: 1.25 fs for the intramolecular forces, 2.5 fs for the intermolecular forces, and simulation data were collected every 100 ps. Analysis of MD data was conducted using pre-defined macro (md_analyze, and md_analyzebindenergy) within YASARA package.

2.4. NMR experiment preparations

^{1}H-NMR spectra were obtained by using a Bruker Advance 600 Hz spectrometer (Germany) with a 5 mm probe in DMSO-d6 at 25 ℃. For Job's plot, the total concentration constants at 10 mM, and different volumes of 10 mM solutions of CNMA and CDs were mixed to obtain the ^{1}H NMR spectra. To determine the apparent binding constant (Scott's plot), constant CDs (2 mM) were mixed with different concentrations of CNMA to attain final CNMA/CDs ratios ranging from 0.0 to 4.0. All samples were interacted to equilibrate before the measurement. 2D ROESY was recorded by a Bruker Advance 600 Hz spectrometer (Germany) at 25 ℃ with a mixing time of 300 ms.

2.5. Characterization of inclusion complexes

The Fourier transform infrared (FT-IR) spectra of CNMA, CDs, and their complexes were recorded on a Nicolet 6700 spectrometer (Thermo Fisher Scientific, USA) at a scanning scope ranging from 4000 cm^{-1} to 400 cm^{-1}. The spectra were obtained by averaging 64 scans with a resolution of 4 cm^{-1}. Potassium bromide palettes were used for all spectra.

Differential scanning calorimetry (DSC) curves were recorded with a TA Q200 thermal analyzer (TA Instruments Co., New Castle, DE, USA) in the range of -50 ℃ to 200 ℃ with the heating rate of 10 ℃/min. Thermogravimetric analysis (TGA) was conducted using a thermogravimetric analyzer (TG 209F1 Iris, NETZSCH, Germany) from 30 ℃ to 400 ℃. The heating rate was 10 ℃/min. All samples were sealed in closed alumina crucibles with an empty reference pan under nitrogen flow.

Scanning electron microscopy (SEM) images of the complexes were examined by a JSM-7500F scanning electron microscope (JEOL, Japan). The samples were sputter-coated with a thin gold layer prior to analysis at 5.0 kV.

2.6. ITC analysis

ITC measurements were performed at 298 K using an ITC200 isothermal titration calorimeter (MicroCal; USA). A 2 mM CNMA solution was placed in a sample cell and titrated by 20 mM CD solution at 500 rpm and at 25 ℃. Twenty successive 2 μL aliquot injections (with an initial injection of 0.4 μL) were conducted with a 40 μL auto-syringe filled with CDs. All solutions were degassed before

measurement to eliminate air bubbles. The resulting corrected injection heats were plotted through model-fitting by using the MicroCal Origin software provided with the instrument. Each experiment was performed in triplicates.

2.7. Encapsulation efficiency, solubility, and dissolution tests

Given that the filter residue reflects the amount of unbound CNMA in the inclusion complex, the encapsulation efficiency of CNMA in the complexes was calculated by the following formula in triplicates:

$$\text{Encapsulation efficiency (\%)} = \frac{\text{Total amount of drug} - \text{Amount of unbound drug}}{\text{Total amount of drug}} \times 100 \quad (1)$$

The water solubility of the complex was evaluated by preparing a saturated solution (Huang et al., 2014). The test was conducted by adding excess CNMA into CD aqueous solutions (0–20 mM), which was then stirred for 24 h at 25 ℃ to achieve equilibrium. The solutions were filtered through a 0.45 μm hydrophilic membrane and then detected at 280 nm using a UV spectrophotometer (TU-1901, Beijing Purkinje General Instrument Co., Ltd., China) after being appropriately diluted. Each experiment was repeated thrice.

In vitro dissolution analyses were performed using a ZRC-8D dissolution tester (Chuangxing, Tianjin, China) with the rotate speed of 100 rpm at 37 ℃. Powdered samples (30 mg) of CNMA and inclusion complexes containing 30 mg of CNMA were separately added to tri-distilled water (1000 mL) at the same time. Aliquots (5 mL) of the sample solutions were removed at every fixed time, and filtered through a

0.45 μm hydrophilic membrane. An equal amount of water was replenished in a timely manner to maintain the solvent volume and avoid the dilution effect. All samples were diluted appropriately to measure the concentration with a UV spectrophotometer.

3. Results and discussion

3.1. Theoretical analysis of the formation process of inclusions

Computer simulation can provide insight into the inclusion between guests and hosts, and verify the experimental results in theory (Chen, Chang, & Gilson, 2004; Yang et al., 2017). In the present work, molecular docking studies were conducted to obtain a visual image of the inclusion of CNMA with CDs (**Fig. 2A**). The benzene ring of CNMA inserted into the cyclodextrin cavity, and bound with the primary hydroxyl groups of CD molecules through hydrophobic effect. Hydrogen bonding was formed between the carbonyl moiety and hydroxyls of β-CD to stabilize the inclusion structure. Thus, the shape and structure of CDs can suitably accommodate guest molecules to form a clathrate structure.

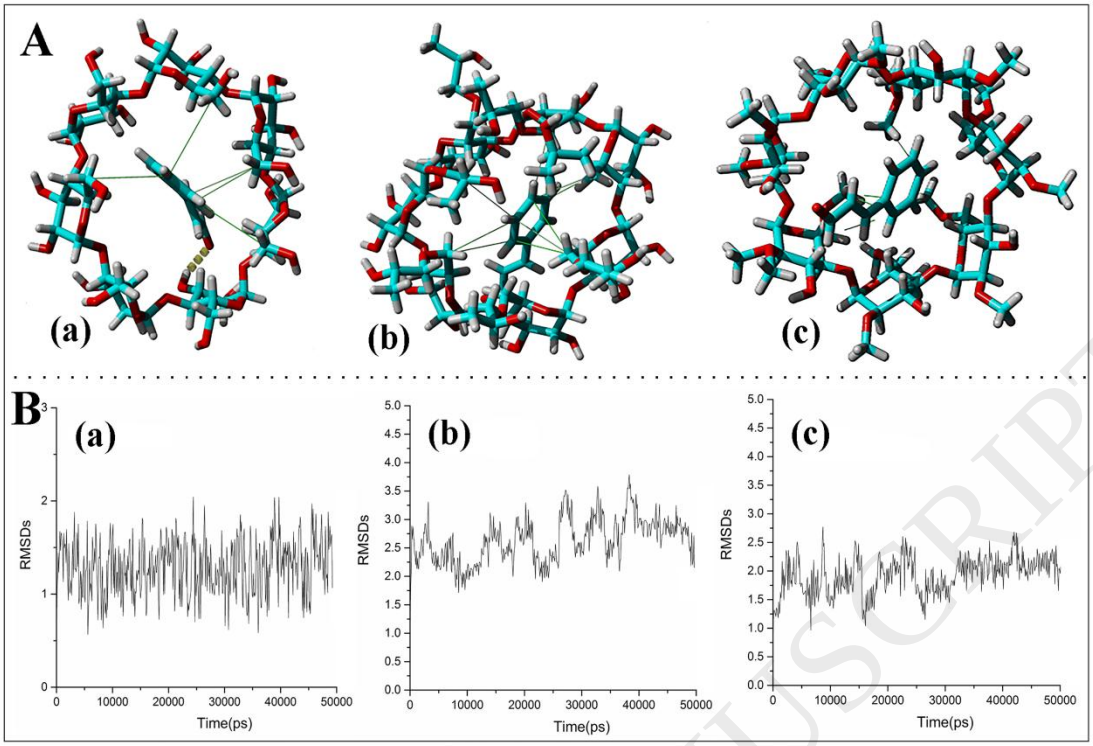

Fig. 2. (A) Representative docking conformations of **(a)** CNMA-β-CD, **(b)** CNMA-HP-β-CD, and **(c)** CNMA-DM-β-CD system. Hydrophobic effects are signified by green-fine lines, and hydrogen bonds are shown as yellow dash lines. **(B)** RMSDs values of three inclusion systems obtained by molecular dynamical simulations to judge system stability. **(a)** CNMA-β-CD system, **(b)** CNMA-HP-β-CD system, and **(c)** CNMA-DM-β-CD system.

In order to predict the stoichiometric ratio between CNMA and CDs, 1:1 and 1:2 clathrate structures were built by molecular docking to perform molecular dynamics simulations (MD). The MD was performed within the most optimal conformation with pH (7.4), temperature (298K), and water solvent. In 1:2 inclusion models (**Fig. S1**), the structure of a 1:2 inclusion is unstable. The inclusion model became 1:1

stoichiometric ratio with the passage of time, resulting in a stable binding structure. However, the inclusion complexes with a 1:1 stoichiometry were stable in MD process (**Fig. S2**). Thus, the host and guest molecules were likely to be a 1:1 clathrate structure.

The inclusion complexes with a 1:1 stoichiometry were further analyzed for obtaining more detailed kinetic information. The root mean square deviation (RMSD) is an index that measures the structural drift from the initial coordinates and the atomic fluctuation in the process of MD simulation (Fujiwara, & Amisaki, 2006). The RMSD values in CNMA with β-CD, HP-β-CD, DM-β-CD systems reached plateau at about 50 ps, 40 ns, and 33 ns, respectively (**Fig. 2B**). The RMSD values calculated from the trajectory data were 1.36±0.58, 2.85±0.22, and 2.16±0.35 Å for β-CD, HP-β-CD, DM-β-CD systems, respectively. Hence, CNMA-β-CD system exhibited the smallest atomic fluctuation. And, the binding energy simulations revealed that the average binding energy of the three inclusion systems followed the order: CNMA-DM-β-CD > CNMA-HP-β-CD > CNMA-β-CD (**Table 1**), and the binding energy of the systems reached balance at 50 ns indicating that the inclusion system reached a stable state (**Fig. S3**). The binding energy results exhibited that the modification of the group could improve the inclusion capacity of β-CD (Zhang et al., 2017).

Table 1 Information obtained from molecular dynamics simulations of free CNMA, free CDs, and inclusion complexes after equilibrium was achieved (50 ns).

System	Average binding energy (KJ/mol)	Bond energy (KJ/mol)	Coulomb (KJ/mol)	VdW (KJ/mol)
CNMA	--	--	-90463	13035
β-CD	--	12495	-92018	12655
HP-β-CD	--	13953	-90818	12333
DM-β-CD	--	14510	-89269	12360
CNMA-β-CD	38.38	12549	-91948	12542
CNMA-HP-β-CD	41.87	14107	-90442	12188
CNMA-DM-β-CD	60.48	14549	-88925	12232

In order to insight into the binding properties and the system stabilities, a detailed analysis was conducted on the MD data (**Table 1**). The results showed that the bond energy was maximal in DM-β-CD inclusion, implying that CNMA had the strongest bonding force in DM-β-CD inclusion. Moreover, there are intermolecular forces on all atoms, and the perturbation of the Coulomb and Van der Waals (VdW) interaction also revealed the changes of the simulation system. Coulomb force is a very important part of the force field between charged atoms. The strong Coulomb force indicated a strong electrostatic force and a compact structure in inclusion system (CNMA-DM-β-CD > CNMA-HP-β-CD > CNMA-β-CD) compared with free CDs and CNMA. The VdW force is a parameter that can reflect the melting points of the compound (Rao & Sunkada, 2007). Thus, inclusion complex should have a higher melting point, which was confirmed by thermal analysis.

Structural information could also gain from the molecular dynamics simulations. To visualize the structural deviations of the complex, no free water was retained in the cavity after complexation with CNMA (**Fig. S4**). As shown in **Fig. S2,** the trajectory analysis showed that the simulated configurations were structurally similar to the initial form, implying that CNMA steadily bound with CDs. The benzene ring moiety of CNMA consistently remained in the hydrophobic cavity of CDs, and this finding agreed with the docking results. Slight changes in the CD structure were observed in β-CD and DM-β-CD, whereas a slightly more evident change was noted in HP-β-CD, which indicated that CNMA-HP-CD system was perturbed.

3.2. Characterization of inclusion complex by NMR spectroscopy

3.2.1. ^{1}H NMR experiments

In this work, the formation of CNMA-CDs inclusion complex was clearly demonstrated by NMR, and the process of inclusion was elucidated preliminarily. The ^{1}H NMR spectra of CNMA in the absence and presence of CDs are presented in **Fig. 3**. The hydrogen chemical shift (δ) and chemical shift differences (Δδ) of CDs and CNMA were shown in Table 2 and Table S1, respectively. In Table 2, inclusion with CNMA exhibited small changes in both β-CD and HP-β-CD, and a significant effect on the chemical shifts of protons of DM-β-CD. The chemical shift of H3, H5, and H6 protons of CDs were changed obviously, indicating that these protons mainly contributed to the inclusion with CNMA. This result was consistent with the previous

results (Li et al., 2015). The chemical shift of H4,6 and H7 protons of CNMA contributed to the inclusion with CDs due to their evident changes (Table S1). Compared with the free CNMA and CDs, the chemical shifts of the inclusion complexes were observed, which indicated that CNMA had reacted with CDs.

Table 2 Chemical shifts (δ) and chemical shift differences (Δδ) of CDs and their corresponding inclusion complexes with CNMA in DMSO-d6.

Hydrogens		H1	H2	H3	H4	H5	H6	H7	H4,7,8	H9
β-CD	δ	4.809	3.333	4.431	3.284	3.599	3.535	-	-	-
CNMA-β-CD	δ	4.811	3.335	4.435	3.287	3.601	3.537	-	-	-
	Δδ	0.002	0.002	0.004	0.003	0.002	0.002	-	-	-
HP-β-CD	δ	5.695	3.403	4.513	-	3.730	3.593	-	3.204	1.005
CNMA-HP-β-CD	δ	5.692	3.400	4.507	-	3.736	3.590	-	3.205	1.007
	Δδ	-0.003	-0.003	-0.006	-	0.006	-0.003	-	0.001	0.002
DM-β-CD	δ	5.773	3.477	4.720	3.357	3.633	3.379	3.228	-	-
CNMA-DM-β-CD	δ	5.783	3.432	4.773	3.352	3.697	3.557	3.232	-	-
	Δδ	0.010	-0.045	0.053	-0.005	0.064	0.178	0.004	-	-

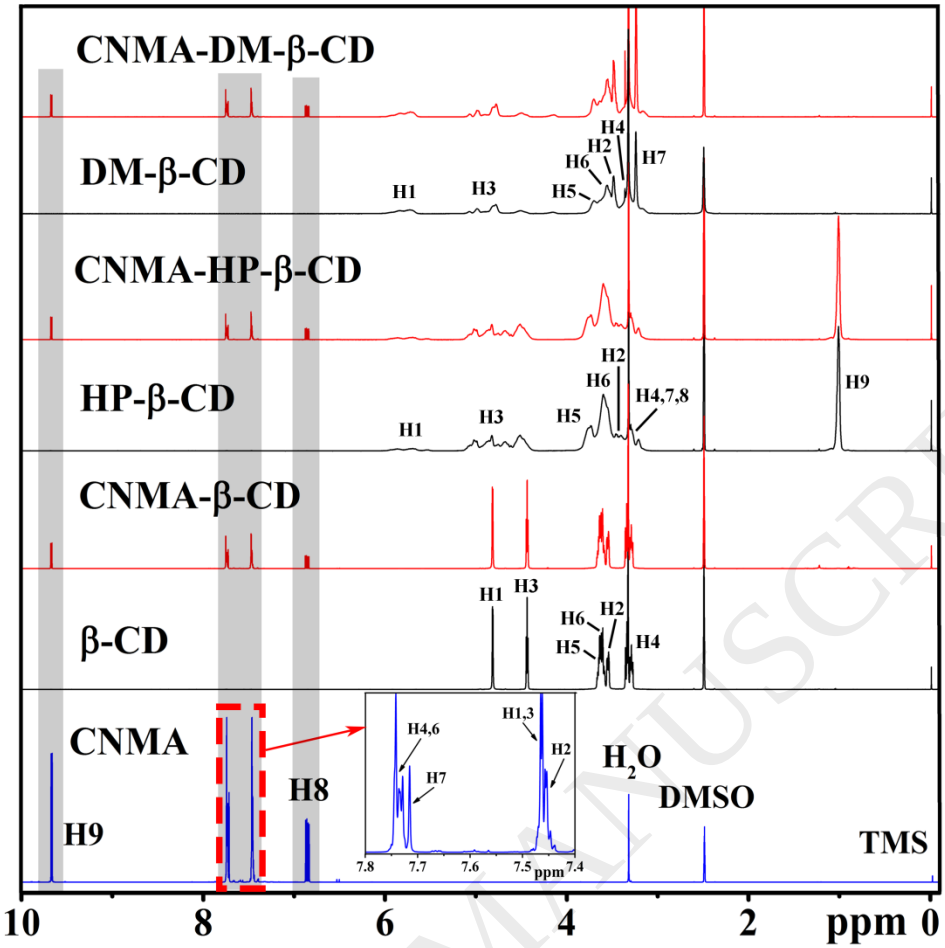

Fig. 3. ^{1}H NMR spectrum of pure CNMA, pure CDs, and inclusion complexes in DMSO-d_6 at room temperature.

3.2.2. Inclusion mode of the inclusion complex

Job's plot was performed to judge the stoichiometry of the inclusion complex between CNMA and CDs (Yee et al., 2017). **Fig. 4A** showed the chemical shifts of H-5 (CDs) for a CD mole fraction (r_{CD}) ranging from 0.0 to 1.0. The observed significant chemical shift was due to the formation of an inclusion complex. It was noteworthy that the shapes of the Job's plots were not symmetrical and the maximum chemical shift difference was 0.4 ~ 0.5, which indicated that the complex of CNMA

with CDs could be a co-existing mixture through 1:1 and 1:2 stoichiometry (Huang, 1982). However, it had been proved that a 1:2 stoichiometry complex was unstable and negligible by the molecule docking results, thus, a 1:1 stoichiometry complex was chosen as a stable state.

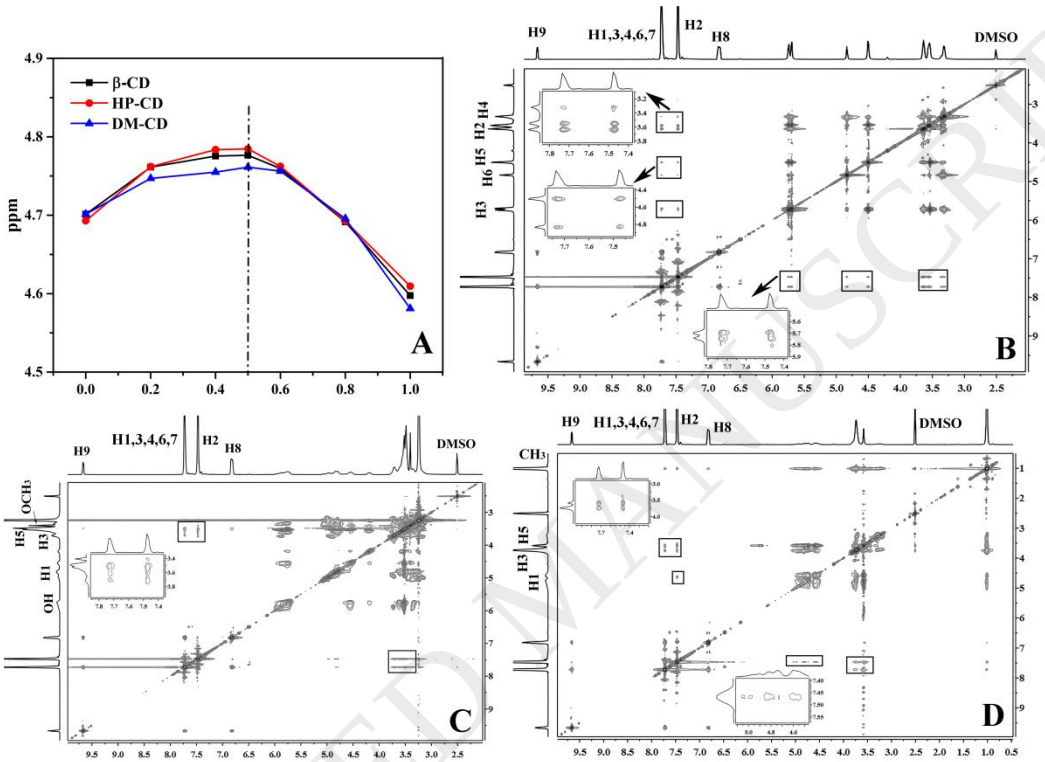

Fig. 4. (A) Job's plot of three inclusion systems. 2D ROESY spectra of **(B)** CNMA-β-CD, **(C)** CNMA-HP-β-CD, and **(D)** CNMA-DM-β-CD system.

3.2.3. Inclusion ability of the inclusion complex

The apparent binding constant (K_b) can be calculated according to the Scott's plot when the guest and the host form a 1:1 inclusion (Choi et al., 2017)

$$\frac{[CNMA]}{\Delta\delta_{obs}} = \frac{[CNMA]}{\Delta\delta_{max}} + \frac{1}{K_b \Delta\delta_{max}} \quad (2)$$

where $\Delta\delta_{obs}$ is the observed chemical shift difference of CD protons with and

without CNMA, and $\Delta\delta_{max}$ is the chemical shift difference at saturation. The results fitted by Eq. 2 were shown in **Fig. 5**. According to the slope and intercept, the apparent binding constants of the three systems could be obtained as follows: H5 (2930 M^{-1}) ≈ H6 (2915 M^{-1}) > H3 (1409 M^{-1}) > H2 (493 M^{-1}) in CNMA-β-CD system, H5 (16754 M^{-1}) > H9 (3652 M^{-1}) > H2 (2829 M^{-1}) > H3 (1125 M^{-1}) in CNMA-HP-β-CD system, and H6 (17522 M^{-1}) > H5 (3300 M^{-1}) > H7 (2658 M^{-1}) > H2,4 (1825 M^{-1}) in CNMA-DM-β-CD system. The inclusion ability followed the ordered with DM-β-CD > HP-β-CD > β-CD, and H5 and H6 played the main roles in the interaction process. DM-β-CD had the highest binding constant, which was the most suitable for forming a complex with CNMA. These results agreed with the average binding energy obtained from molecular dynamics simulations.

This result can be explained by two possible reasons: one is the cavity size and compact structure of cyclodextrin, and the other one is its hydrophobic nature. For the first reason, given that the guest has a small molecular weight and a plane structure, the modified β-CD cavity structure is more compact and more conducive to an inclusion with the guest. For the second reason, since hydrophobic effect is the main driving force of inclusion, the inclusion ability of methyl modified β-CD is stronger than that modified by hydroxyl, and the hydrophobic group of CNMA is mainly responsible for the combination.

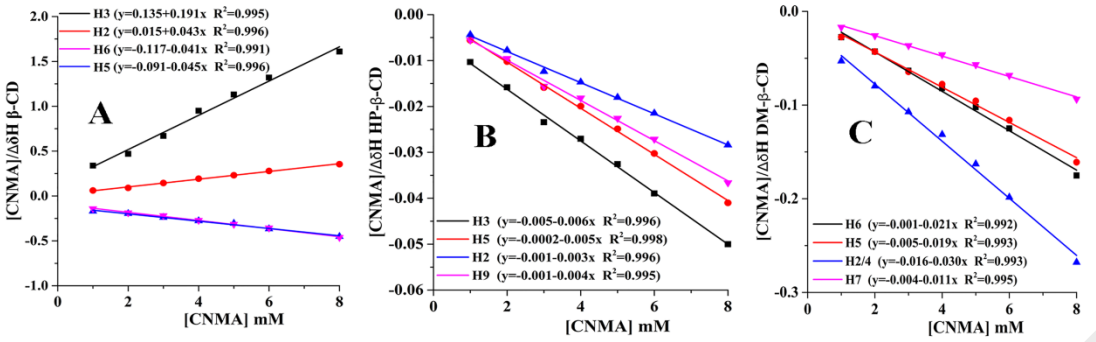

Fig. 5. Scott's plot for three inclusion system with CD concentration set at 2 mM and variable CNMA concentration at pH 7.4 at room temperature. **(A)** is for CNMA-β-CD system. **(B)** is for CNMA-HP-β-CD system. **(C)** is for CNMA-DM-β-CD system.

3.2.4. Structure of the inclusion complex

In order to further identify the structure and inclusion modes of the complexes in the solution, 2D-ROESY was conducted in D_2O at room temperature. The spectra presented the NOE cross-peaks between the protons for spatial contacts within 4 Å (Schneider, Hacket, Rüdiger, & Ikeda, 1998). **Fig. 4** showed the 2D-ROESY spectra of the three systems. In CNMA-β-CD system, the cross peak correlations of H1,2,3,4,6,7 (CNMA) and H2,3,4,5,6 (β-CD) were observed to determine the entire CNMA molecule inserted into the β-CD cavity. H3,5 (DM-β-CD) and H1,3,5 (HP-β-CD) displayed cross peak correlations with H1,2,3,4,6,7 (CNMA), indicating that the CNMA molecule penetrated the hydrophobic cavity. This inclusion mode wherein the entire guest molecule interacted with CDs may be due to two possible reasons. One is the small molecular weight of CNMA. The other is that aromatic compounds typically have a pronounced interaction with the CD hydrophobic cavity

because of the aromatic ring (Schneider, Hacket, Rüdiger, & Ikeda, 1998). These results confirmed the interactions between the guest and host molecules and that the benzene ring of CNMA plays an important role in inserting into the hydrophobic cavities of CDs.

3.3. Solid-state characterization of inclusion complexes

3.3.1. FT-IR spectra

Changes in the FT-IR spectra may be provide insight into the potential guest–CDs interaction (Almarzouqi, Elwy, Shehadi, & Adem, 2009). The strong peak of CNMA at ~1620 cm^{-1}, which was attributed to the stretching vibrations of C=O groups, appeared in the inclusion complex (**Fig. 6A**). However, several peaks of the vibrations of the aromatic ring framework around at 1700 - 2000 cm^{-1} and two peaks of the stretching vibrations of C-H of the aldehyde group at ~2700 and ~2800 cm^{-1} completely disappeared compared with physical mixture in the three systems. Thus, the inclusion complexes formed between CNMA and CDs, with the aromatic moiety and aldehyde group of CNMA included in the CD cavities.

3.3.2. DSC and TGA analysis

DSC and TGA are useful tools for identifing the interaction by using thermograms (Maeda, Yu, & Nakayama, 2013; Marques, Hadgraft, & Kellaway, 1990; Taupitz, Dressman, Buchanan, & Klein, 2013). The endothermic peak around -19 ℃, which is the melting point of CNMA, was observed and increased to a higher temperature in the inclusion complex in DSC curves (**Fig. 6B**). The inclusion process

improves the thermal stability of CNMA. In **Fig. 6C,** the TGA results of CNMA and its inclusion complex were shown. The mass loss of less than 100 °C can be associated to water loss of CDs. The significant mass loss around 130 °C in the HP/DM-β-CD inclusions was mainly due to the evaporation of the CNMA from the inclusion complex. Then, the decomposition of CDs occurred at a higher temperature. These changes in the curves confirmed the formation of inclusion complexes. These results indicated that the thermal stability of CNMA was modified after complexation with CDs, particularly in β-CD. The results agreed with the VdW forces that found in molecular dynamics simulation results.

3.3.3. SEM

SEM is an ideal method for measuring surface morphology, including particle size, surface roughness, and surface texture of substances (Gong et al., 2016; Tang et al., 2017). The SEM images of the samples are displayed in **Fig. S5**. The size and surface morphologies were changed by the inclusion. The CNMA-β-CD complexes showed a relatively more homogeneous shape with a rough and fluffy texture, an irregular surface, and smaller sizes. Morphological analysis revealed that CNMA-HP-β-CD and CNMA-DM-β-CD displayed an irregular blocky form, which was markedly different from the shapes of free CDs. The morphological differences of the materials confirmed the formation of a new solid phase.

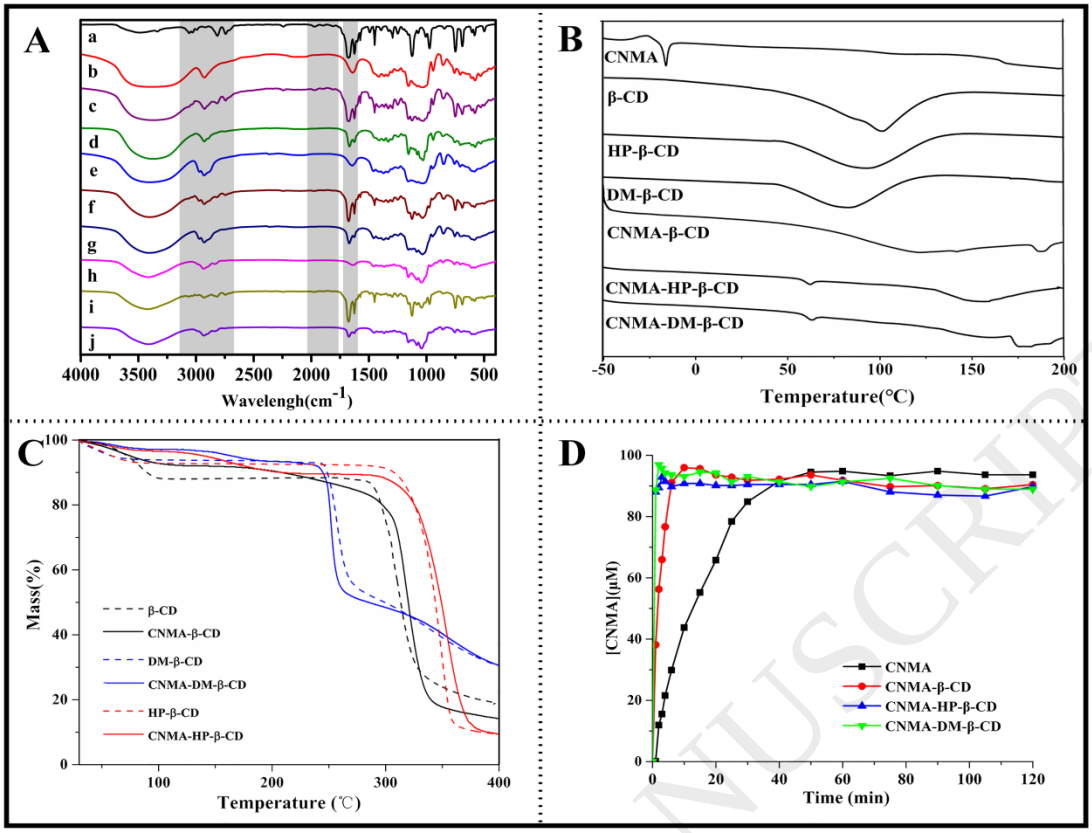

Fig. 6. (A) IR spectra of (a) pure CNMA, (b) pure β-CD, (c) physical mixture of CNMA and β-CD, (d) CNMA-β-CD, (e) pure HP-β-CD, (f) physical mixture of CNMA and HP-β-CD, (g) CNMA-HP-β-CD, (h) pure DM-β-CD, (i) physical mixture of CNMA and DM-β-CD, and (j) CNMA-DM-β-CD. **(B)** DSC curves of pure CNMA, pure CDs, and inclusion complex. **(C)** TGA curves of pure CDs and inclusion complex. **(D)** Release curves of CNMA in the pure state and inclusion complex in water at 37℃.

3.4. Thermodynamic properties of the inclusion

Detailed thermodynamic information, including the stability constant of complex (K), enthalpy change (ΔH), entropy change (ΔS), and changes of Gibbs free energy

(ΔG), were obtained by using the ITC method (Kitamura, Nakatani, Takaha, & Okada, 1999). The thermodynamic parameters were calculated by the van't Hoff equation:

$$\Delta G = -RT\ln K \quad (3)$$

$$\Delta G = \Delta H - T\Delta S \quad (4)$$

Fig. 7 showed the isothermal calorimetry titration curves of CNMA with three types of CDs. Results obtained from the nonlinear least-squares fitting and the aforementioned equations were presented in **Fig. 7**. ΔG and ΔH were negative in all three systems, demonstrating that the inclusion processes were spontaneous, exothermic (Belica et al., 2014). Moreover, the positive ΔS indicated that the degree of disorder was larger in the system, which contribute to the spontaneity of the reactions (Passos et al., 2013). The inclusion process were driven by both enthalpy and entropy, however, the enthalpic effects of binding dominate over entropic effects because of $|\Delta H| > |T\Delta S|$ (Belica et al., 2014). The binding constant (K) followed the order of β < HP < DM in the inclusion progress. A larger binding constant corresponded to an easier inclusion. The results were consistent with Scott's plot. The slight differences in the data may be due to the differences in sample preparation (deuterium generation reagent etc.) and instruments.

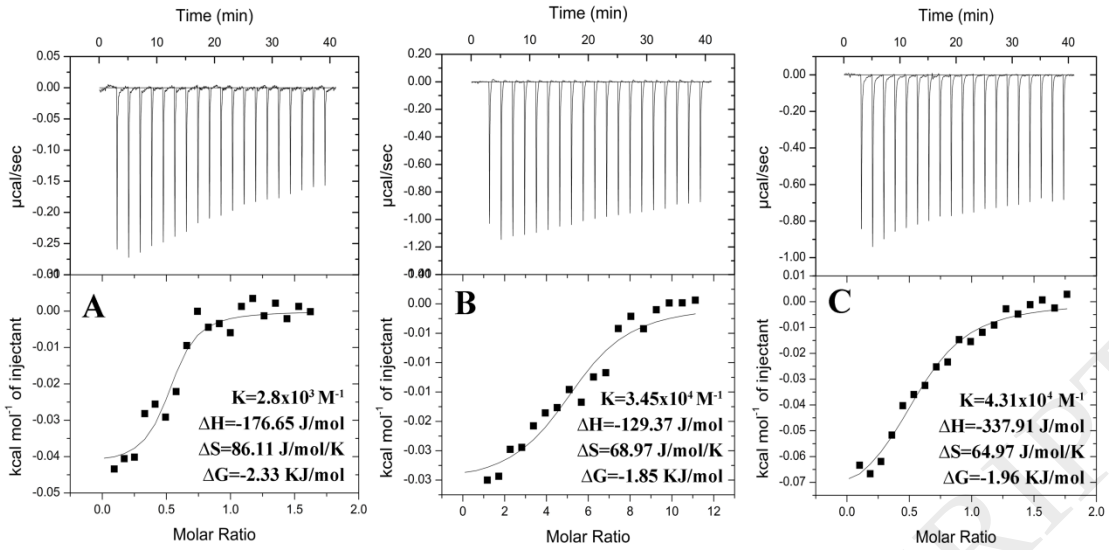

Fig. 7. Isothermal calorimetry titration curves of CNMA with **(A)** CNMA-β-CD, **(B)** CNMA-HP-β-CD, and **(C)** CNMA-DM-β-CD at 298 K.

3.5. Analysis of encapsulation efficiency, solubility, and dissolution

The encapsulation efficiency and solubility enhancements in water were summarized in **Table 3**. The encapsulation abilities for CNMA followed the order: β-CD < HP-β-CD < DM-β-CD, and HP-β-CD and DM-β-CD showed similar encapsulation abilities. β-CD slightly affected the solubility of CNMA, and DM-β-CD increased the solubility of CNMA to a greater extent than HP-β-CD did. The dissolution rates of all samples were high. Free CNMA dissolved slowly (90% after 40 min) because of its poor water solubility (**Fig. 6D**). All samples demonstrated a very high cumulative release percentage of over 90%. The reason for the increased solubility and accelerated dissolution rate after inclusion was the structural features of the CDs, which include a hydrophobic cavity and a hydrophilic outer surface.

Table 3 Encapsulation efficiency and solubility enhancement of inclusion complexes.

Inclusion complex	Solubility in water (mM)	Encapsulation efficiency（%）
CNMA	0.675±0.003	--
CNMA-β-CD	1.593±0.004	29.346±0.873
CNMA-HP-β-CD	15.864±0.008	46.477±0.748
CNMA-DM-β-CD	21.127±0.006	53.623±1.022

Values are presented as mean ± SD (n = 3).

4. Conclusion

In this work, the structural model and binding mechanism of the inclusion complex CNMA-CDs were gained from computer simulation and correlated with experimental data. CNMA and CDs formed a 1:1 inclusion complex. DM-β-CD showed the strongest binding ability in the inclusion process with CNMA. The benzene ring of CNMA inserted into the hydrophobic cavities of CDs, and H5,6 of CDs and the benzene ring of CNMA played the main roles in the interaction, which were the primary structure features in CNMA-CDs inclusion process. The complexes of CNMA with CDs showed improved solubility, stability, and dissolution rate compared with the pure drug. The research provides some theoretical and experimental information for the application of CNMA and its inclusion complexes.

Acknowledgments

This work was supported by the Large-scale Science Instrument Shareable Platform Construction of Sichuan Province (Grant No. 2015JCPT0005-15010102) and the

Large-scientific Instruments Sharing Platform Ability Construction of Sichuan Province (Grant No. 2016KJTS0037).

References

Abdolmaleki, A., Ghasemi, F., & Ghasemi, J. B. (2017). Computer-aided drug design to explore cyclodextrin therapeutics and biomedical applications. *Chemical Biology & Drug Design, 89*(2), 257-268.

Almarzouqi, A. H., Elwy, H. M., Shehadi, I., & Adem, A. (2009). Physicochemical properties of antifungal drug-cyclodextrin complexes prepared by supercritical carbon dioxide and by conventional techniques. *Journal of Pharmaceutical & Biomedical Analysis, 49*(2), 227-233.

Anand, P., Murali, K. Y., Tandon, V., Murthy, P. S., & Chandra, R. (2010). Insulinotropic effect of cinnamaldehyde on transcriptional regulation of pyruvate kinase, phosphoenolpyruvate carboxykinase, and GLUT4 translocation in experimental diabetic rats. *Chemico-biological interactions, 186*(1), 72-81.

Belica, S., Jeziorska, D., Urbaniak, P., Buko, V. U., Zavodnik, I. B., & Pałecz, B. (2014). Calorimetric and spectroscopic characterization of complexes between β-cyclodextrin or heptakis (2,6-di-O-methyl)-β-cyclodextrin and sertraline hydrochloride in aqueous solution. *Journal of Chemical Thermodynamics, 70*(70), 160-167.

Carrier, R. L., Miller, L. A., & Ahmed, I. (2007). The utility of cyclodextrins for enhancing oral bioavailability. *Journal of Controlled Release, 123*(2), 78-99.

Castro, D. O., Tabary, N., Martel, B., Gandini, A., Belgacem, N., & Bras, J. (2016). Effect of different carboxylic acids in cyclodextrin functionalization of cellulose nanocrystals for prolonged release of carvacrol. *Materials Science & Engineering C, 69*, 1018-1025.

Chen, W., Chang, C. E., & Gilson, M. K. (2004). Calculation of Cyclodextrin Binding

Affinities: Energy, Entropy, and Implications for Drug Design. *Biophysical Journal, 87*(5), 3035-3049.

Chun, J. Y., Jo, Y. J., Bjrapha, P., Choi, M. J., & Min, S. G. (2015). Antimicrobial Effect of α- or β-Cyclodextrin Complexes with Trans-Cinnamaldehyde Against Staphylococcus aureus and Escherichia coli. *Drying Technology, 33*(3), 377-383.

Fernándezgarcía, E., & Pérezgálvez, A. (2017). Carotenoid:β-cyclodextrin stability is independent of pigment structure. *Food chemistry, 221*, 1317-1321.

Ferro, M., Castiglione, F., Pastori, N., Punta, C., Melone, L., & Panzeri, W. (2017). Dynamics and interactions of ibuprofen in cyclodextrin nanosponges by solid-state NMR spectroscopy. *Beilstein Journal of Organic Chemistry, 13*, 182-194.

Fujiwara, S., & Amisaki, T. (2006). Molecular dynamics study of conformational changes in human serum albumin by binding of fatty acids. *Proteins-structure Function & Bioinformatics*, 64(3), 730–739.

Gong, L., Li, T., Chen, F., Duan, X., Yuan, Y., Zhang, D., & Jiang, Y. (2016). An inclusion complex of eugenol into β-cyclodextrin: Preparation, and physicochemical and antifungal characterization. *Food chemistry, 196*, 324-330.

Huang, C. Y. (1982). Determination of binding stoichiometry by the continuous variation method: the job plot. *Methods in Enzymology, 87*(87), 509-525.

Huang, J., Wang, S., Luo, X., Xie, Y., & Shi, X. (2007). Cinnamaldehyde reduction of platelet aggregation and thrombosis in rodents. *Thrombosis Research, 119*(3), 337-342.

Huang, Z., Tian, S., Ge, X., Zhang, J., Li, S., & Li, M. (2014). Complexation of chlorpropham with hydroxypropyl-β-cyclodextrin and its application in potato sprout inhibition. *Carbohydrate Polymers, 107*(107), 241-246.

Chou, J.M., Park, K., Lee, B., Jeong, D., Dindulkar, S.D., & Choi, Y. (2017). Solubility and bioavailability enhancement of ciprofloxacin by induced oval-shaped mono-6-deoxy-6-aminoethylamino-β-cyclodextrin. *Carbohydrate Polymers, 163*, 118-128.

Kitamura, S., Nakatani, K., Takaha, T., & Okada, S. (1999). Complex formation of large‐ring cyclodextrins with iodine in aqueous solution as revealed by isothermal titration calorimetry. *Macromolecular Rapid Communications, 20*(12), 612-615.

Krieger, E., Darden, T., Nabuurs, S. B., Finkelstein, A., & Vriend, G. (2004). Making optimal use of empirical energy functions: Force‐field parameterization in crystal space. *Proteins-structure Function & Bioinformatics, 57*(4), 678‐683.

Li, S., Wang, L., Jiang, J., Tang, P., Wang, Q., Wu, D., & Li, H. (2015). Investigations of bisacodyl with modified β-cyclodextrins: Characterization, molecular modeling, and effect of PEG. *Carbohydrate Polymers, 134*, 82-91.

Liscieplak, A., Sitkowski, J., & Kolodziejski, W. (2014). Comparative proton nuclear magnetic resonance studies of amantadine complexes formed in aqueous solutions with three major cyclodextrins. *Journal of Pharmaceutical Sciences, 103*(1), 274-282.

Maeda, H., Yu, O., & Nakayama, H. (2013). Inclusion complexes of melatonin with modified cyclodextrins. *Journal of Inclusion Phenomena & Macrocyclic Chemistry, 78*(1-4), 217-224.

Makwana, S., Choudhary, R., Dogra, N., Kohli, P., & Haddock, J. (2014). Nanoencapsulation and immobilization of cinnamaldehyde for developing antimicrobial food packaging material. *LWT - Food Science and Technology, 57*(2), 470-476.

Marques, H. M. C., Hadgraft, J., & Kellaway, I. W. (1990). Studies of cyclodextrin inclusion complexes. I. The salbutamol-cyclodextrin complex as studied by phase solubility and DSC. *International Journal of Pharmaceutics, 63*(3), 259-266.

Nagle, A. A., Gan, F. F., Gavin, J., Choon-Leng, S., Geoffrey, W., & Eng-Hui, C. (2012). Induction of Tumor Cell Death through Targeting Tubulin and Evoking Dysregulation of Cell Cycle Regulatory Proteins by Multifunctional Cinnamaldehydes. *PloS one, 7*(11), e50125.

Passos, J. J., Sousa, F. B. D., Mundim, I. M., Bonfim, R. R., Melo, R., & Viana, A. F., et al. (2013). Double continuous injection preparation method of cyclodextrin

inclusion compounds by spray drying. *Chemical Engineering Journal, 228*(28), 345-351.

Pessine, F. B. T., Calderini, A., & Alexandrino, G. L. (2012). Review: Cyclodextrin Inclusion Complexes Probed by NMR Techniques. *InTech,* 237-264

Ponce Cevallos, P. A., Buera, M. P., & Elizalde, B. E. (2010). Encapsulation of cinnamon and thyme essential oils components (cinnamaldehyde and thymol) in β-cyclodextrin: effect of interactions with water on complex stability. *Journal of Food Engineering, 99*(1), 70-75.

Rao, S. P., & Sunkada, S. (2007). Making sense of boiling points and melting points. *Resonance, 12*(6), 43-57.

Schneider, H. J., Hacket, F., Rüdiger, V., & Ikeda, H. (1998). NMR Studies of Cyclodextrins and Cyclodextrin Complexes. *Chemical Reviews, 98*(5), 1755-1785.

Tang, P., Yang, H., Tang, B., Wu, D., Du, Q., Xu, K., & Li, H. (2017). Dimethyl-β-cyclodextrin/salazosulfapyridine inclusion complex-loaded chitosan nanoparticles for sustained release. *Carbohydrate Polymers, 156,* 215-222.

Taupitz, T., Dressman, J. B., Buchanan, C. M., & Klein, S. (2013). Cyclodextrin-water soluble polymer ternary complexes enhance the solubility and dissolution behaviour of poorly soluble drugs. Case example: itraconazole. *European Journal of Pharmaceutics & Biopharmaceutics, 83*(3), 378-387.

Tian, Y., Zhu, Y., Bashari, M., Hu, X., Xu, X., & Jin, Z. (2013). Identification and releasing characteristics of high-amylose corn starch-cinnamaldehyde inclusion complex prepared using ultrasound treatment. *Carbohydrate Polymers, 91*(2), 586-589.

Yang, J., Tang, K., Qin, G., Chen, Y., Peng, L., & Wan, X., et al. (2017). Hydrogen bonding energy determined by molecular dynamics simulation and correlation to properties of thermoplastic starch films. *Carbohydrate Polymers, 166*, 256-263.

Yee, E. M., Hook, J. M., Bhadbhade, M. M., Vittorio, O., Kuchel, R. P., & Brandl, M., et al. (2017). Preparation, characterization and in vitro biological evaluation of (1:2)

phenoxodiol-β-cyclodextrin complex. *Carbohydrate Polymers, 165*, 444-454.

Zeynep, A., Semran Ipek, K., Engin, D., & Tamer, U. (2016). Quercetin/β-cyclodextrin inclusion complex embedded nanofibres: Slow release and high solubility. *Food chemistry, 197*(Pt A), 864-871.

Zhang, C. L., Liu, J. C., Yang, W. B., Chen, D. L., & Jiao, Z. G. (2017). Experimental and molecular docking investigations on the inclusion mechanism of the complex of phloridzin and hydroxypropyl-β-cyclodextrin. *Food chemistry, 215*, 124-128.